Dalton Transactions

ROYAL SOCIETY OF CHEMISTRY

PERSPECTIVE

View Article Online
View Journal | View Issue

Cite this: *Dalton Trans.*, 2026, **55**, 1958

Alloying-mediated stability enhancement of zinc anodes for high-performance zinc-ion batteries

Pushan Guo, *[a,b,c] Zhihao Dong,[a] Jinrong Qi,[a] Jingjing Yuan, [d] Tao Chen,[e] Yi Zhang*[a] and Linhao Xin[c]

Aqueous zinc-ion batteries (AZIBs) have emerged as a core candidate system for next-generation electrochemical energy storage technologies due to their high safety, low cost, and abundant resources. However, their industrialization process is constrained by key issues, such as zinc dendrite growth, hydrogen evolution reactions, and corrosion loss. Compared with the optimization of electrolyte components, the alloying modulation of the zinc anode represents a more direct strategy to enhance its stability. By introducing heterogeneous metal elements to form alloy phases with zinc, a multi-dimensional synergistic optimization of the electronic structure, crystal growth, and interfacial behavior can be achieved. This perspective systematically summarizes the research progress of the alloying strategy in the modification of zinc anodes for AZIBs and analyzes the core mechanisms of the alloying modulation. In particular, it focuses on regulating the d-band center at the electronic structure level to enhance Zn^{2+} adsorption, inducing the preferential deposition of Zn along the (002) crystal plane, and constructing buffer layers to reduce the electrode reaction activity. Moreover, the formation positions and functional modes of the alloy phases are elaborated. The perspective further points out the current challenges in research and prospects the development directions, aiming to provide theoretical support and technical reference for the design of high-stability zinc anodes and achieve overall performance improvement in AZIBs.

Received 28th October 2025,
Accepted 8th December 2025

DOI: 10.1039/d5dt02588e

rsc.li/dalton

1. Introduction

Aqueous zinc-ion batteries (AZIBs) exhibit irreplaceable application potential in large-scale energy storage, portable electronic devices, and electric vehicles.[1–5] This is attributed to their advantages of high theoretical capacity and low redox potential of metallic zinc, high safety of electrolytes, abundant zinc resources, and low cost.[6–9] As such, AZIBs are regarded as one of the core candidates for next-generation electrochemical energy storage technologies.[10,11] However, the industrialization of AZIBs is still limited by the stability issues of zinc anodes, which essentially stem from the interaction between zinc and the aqueous electrolyte interface.[12–14] At the atomic scale, the disordered diffusion of Zn^{2+} during zinc deposition tends to cause random nucleation growth.[15–18] Particularly in the deep discharge process, the tip effect exacerbates the longitudinal extension of dendrites.[19–21] Sharp dendrites not only pierce the separator and trigger battery short circuits but also increase the specific surface area of the electrode, inducing side reactions.[22–24] At the interface scale, H_2O molecules in the aqueous electrolyte are prone to undergo the hydrogen evolution reaction (HER) on the zinc surface.[25] The generated H_2 bubbles damage the electrode/electrolyte interface contact. Meanwhile, reaction products, such as $Zn(OH)_2$ and $Zn_4(SO_4)(OH)_6{\cdot}xH_2O$, form an insulating passivation layer on the anode surface. This layer hinders ion transport and electron conduction, leading to a sharp drop in the coulombic efficiency and shortened cycle life. These mutually coupled issues have become the core scientific bottlenecks restricting the performance breakthrough of AZIBs.

To address the aforementioned bottlenecks, the scientific community has developed various zinc anode modification strategies (Fig. 1). The evolution of these technical routes shows a trend from macro-regulation to precise interface design.[26–28] The early structural designs of zinc anodes, such as porous zinc and zinc-based composites, alleviate volume expansion by optimizing the electrode's micro-morphology but fail to fundamentally inhibit the dendrite growth and HER.[29,30] As a typical modification approach targeting the interface environment, electrolyte engineering has obvious

[a]*School of Mechanical Engineering and Rail Transit, Changzhou University, Changzhou 213164, China. E-mail: guopushan@cczu.edu.cn*
[b]*School of Materials Science and Engineering, Changzhou University, Changzhou 213164, China*
[c]*Ningbo Guanghua Battery Co., Ltd, Ningbo 315124, China*
[d]*College of Petrochemical Engineering, Changzhou University, Changzhou 213164, China*
[e]*Changzhou Changda Intelligent Manufacturing Technology Co., Ltd, Changzhou 213116, China*

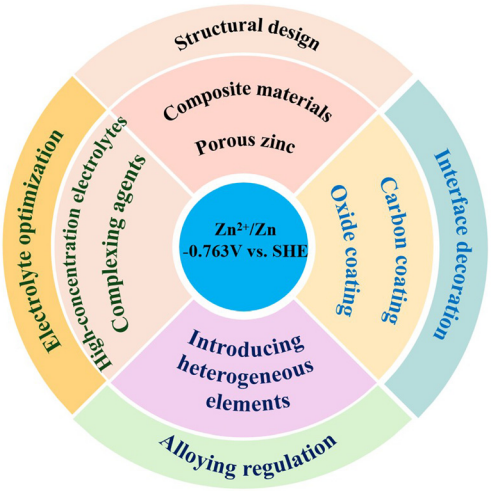

Fig. 1 Modification strategies for zinc anode.

strengths in operational simplicity; adjusting electrolyte components or adding additives can quickly optimize Zn^{2+} deposition behavior without modifying the zinc anode matrix, making it more flexible for short-term performance tuning. For example, electrolyte optimization strategies, including the addition of complexing agents and the construction of high-concentration electrolytes, improve the interface environment, yet these methods suffer from problems like high cost and low ionic conductivity.[31–33] This is in contrast to the alloying modulation strategy for zinc anodes. While electrolyte engineering focuses on regulating the external interface environment, alloying directly modifies the intrinsic properties of the zinc anode, and its improvement effect on anode long-term stability is more durable, which is more suitable for the long-cycle application demands of AZIBs.[34–38] In addition, the interface modification strategies of coating carbon-based or oxide layers could build robust physical barriers.[39–41] However, the poor interfacial adhesion between the coating and the zinc matrix easily causes the coating to peel off and fail during cycling.[42] In contrast, the alloying modulation strategy for zinc anodes achieves the multi-dimensional regulation of electronic structure, crystal growth, and interface behavior by introducing heterogeneous metal elements (*e.g.*, Sn, Bi, Cu, and Ce) into the zinc matrix to form alloy phases.[43–45] Its core advantage lies in altering the intrinsic properties of zinc through atomic-level doping, which fundamentally optimizes zinc deposition kinetics and interface stability.[46–48] Meanwhile, this technology can be implemented through methods such as smelting or electrodeposition, and is easy to industrialize.[49–51] Therefore, this strategy has gradually become the dominant technical route for current zinc anode modification.

In recent years, the zinc alloying strategy for AZIBs has evolved from single-element doping to multi-component design, expanded from bulk alloying to interfacial dynamic alloying, and advanced from basic performance research to the exploration of industrial applications.[52–55] However, current research still faces multiple unresolved scientific and technical bottlenecks. There are inherent differences in the action mechanisms of various heterogeneous elements, and the dynamic evolution laws remain unclear, such as the dissolution and reconstruction of alloy phases during cycling.[56–58] The synergistic effects between alloying and other modification strategies lack in-depth investigation, and controlling component uniformity during large-scale preparation is also quite challenging.[59] These issues not only result in the lack of systematic theoretical support for alloying modulation, but also make it difficult to form unified rules for performance improvement.[60–62]

Based on this, this perspective focuses on the alloying-dominated performance regulation of high-stability zinc anodes for AZIBs. By analyzing the internal mechanism of stable zinc alloy anodes, it elaborates on the technical principles, typical research cases, and performance breakthroughs from five aspects: the *in situ* construction of Zn alloy interface, the scalable fabrication of bulk Zn alloy, the fabrication of composite coating-based Zn anode, the *ex situ* zinc alloy forming fabrication, and the post-treatment modification of zinc anode.[62–64] Finally, it summarizes the challenges of the alloying strategy in terms of compatibility with high-loading cathodes and long-cycle alloy phase, while prospecting directions such as high-throughput computation-assisted alloy design and integrated preparation process development.[65–67] It is expected to provide theoretical support for the precise design of high-stability zinc anodes for AZIBs.

2. Internal mechanism of the stable zinc alloy anodes

The improvement effect of the alloying strategy on the stability of the zinc anodes in AZIBs essentially stems from the synergistic regulatory role in the electronic structure, crystal growth, and interfacial reactions for alloy phases, which are formed by heterogeneous metal elements and zinc. Fig. 2 illustrates the mechanism, strategy, and structural characteristics of zinc alloy anodes.[68–70] From the perspective of electronic structure regulation, the introduction of heterogeneous elements

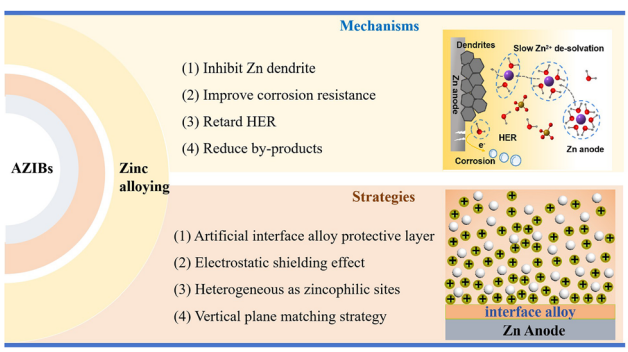

Fig. 2 Mechanisms and strategies of zinc alloy anodes.

changes the electron cloud distribution and d-band center energy of the zinc anode. On the one hand, the electronegativity difference between heterogeneous atoms and zinc atoms induces electron migration toward atoms with relatively high electronegativity, forming local charge-enriched regions.[71–73] This enhances the adsorption capacity of the alloy phases for Zn^{2+} and prevents the disordered aggregation of Zn^{2+} on the anode surface. Notably, a moderate upward shift of the d-band center, which is relative to the Fermi level, strengthens the electronic coupling between metal d-orbitals and Zn^{2+} valence orbitals, optimizing Zn^{2+} adsorption energy to promote ordered deposition on low-energy crystal planes while reducing Zn^{2+} reduction barriers for accelerated deposition kinetics.[74] On the other hand, the moderate upward shift of the d-band center reduces the reduction energy barrier of Zn^{2+}, accelerates zinc deposition kinetics, and simultaneously weakens the bonding strength between H^+ and the anode surface; this is attributed to the competitive adsorption effect between Zn^{2+} and H^+ on the alloy phase surface. The enhanced Zn^{2+} adsorption affinity of the alloy phase occupies active sites that would otherwise be available for H^+ adsorption and reduction, fundamentally inhibiting the HER.[75–77] Moreover, the modified electronic structure of the alloy phase elevates the HER onset potential and increases the reaction energy barrier for $H^+ \rightarrow H_2$ conversion, further suppressing hydrogen gas generation during long-term cycling.

At the level of crystal growth guidance, the formation of alloy phases provides a preferential growth template for zinc deposition. Most alloy phases (*e.g.*, Zn–Sn and Zn–Ce) formed by heterogeneous elements (*e.g.*, Sn and Ce) and zinc have a crystal structure with a high matching degree to the (002) close-packed crystal plane of zinc.[78–82] Specifically, the lattice parameters and atomic stacking mode of these alloy phases exhibit minimal lattice mismatch with Zn (002) planes, for example, Zn–Sn intermetallics with tetragonal structures and Zn–Ce compounds with hexagonal symmetries, which enables them to act as epitaxial substrates for Zn deposition. During the nucleation stage, Zn^{2+} tends to adsorb onto these alloy-phase surfaces due to the reduced interfacial energy caused by lattice matching, preferentially initiating deposition at sites aligned with the (002) crystal orientation of Zn. As deposition proceeds, the alloy phase template constrains the growth direction of the Zn atoms, guiding their stacking along the (002) plane to form a continuous, layered structure while suppressing the lateral growth of the (100) and (101) planes that are thermodynamically prone to dendrite formation. As a low-surface-energy crystal plane of zinc, the (002) plane has a dense atomic arrangement, which can effectively reduce the active sites for dendrite nucleation and form a dense and uniform zinc deposition layer.[83–85] This dense deposition layer further acts as a physical barrier to inhibit the direct contact between the fresh Zn substrate and the electrolyte, reducing the chance of Zn oxidation and electrolyte decomposition that lead to the byproduct formation of $Zn(OH)_2$ and $Zn_4(SO_4)(OH)_6{\cdot}xH_2O$. From the perspective of interfacial reaction inhibition, alloy phases can construct a stable interfacial buffer layer. First, the chemical stability of alloy phases is generally higher than that of pure zinc, which can reduce the reaction activity between the anode and the aqueous electrolyte and decrease the formation of corrosion products, such as $Zn(OH)_2$ and $Zn_4(SO_4)(OH)_6{\cdot}xH_2O$. Second, some alloy phases (*e.g.*, Zn–Co and Zn–Bi) possess excellent ion conductivity, which can form uniform transport channels for Zn^{2+} on the surface of an anode.[86–88] This avoids the tip effect caused by the uneven flux distribution of Zn^{2+} and further inhibits dendrite growth.

3. Alloying modulation strategies for zinc anodes

Based on differences in the formation position, structural characteristics, and action mechanism of metal phases, the zinc alloying modulation strategies can be further divided into five categories (Fig. 3). The first one is the dynamic alloying modulation focusing on the interface region. It generates alloy interface phases *in situ* to supplement zinc-philic sites in real time and guide the uniform deposition of zinc.[89] The second one is the alloy optimization modulation for the zinc bulk phase. It utilizes processes such as smelting and melting to uniformly dope heterogeneous elements into the zinc matrix, constructing an integrated alloy structure without interface defects.[90–92] The third one is the modulation of the composite protective layer construction that integrates the advantages of multiple components. It combines alloy phases with materials like polymers and ceramics to form a dual barrier for kinetic regulation and physical protection.[93]

3.1 *In situ* construction of Zn alloy interface

This strategy focuses on dynamic regulation at the anode interface, *in situ* generating the interface phases of Zn alloy to dynamically supplement zinc-philic active sites and guide zinc deposition along the (002) close-packed crystal plane. Its core lies in the real-time modulation of the alloy phases to regulate

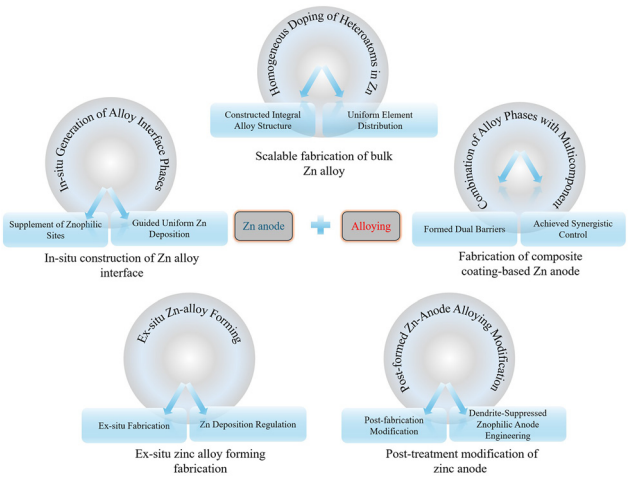

Fig. 3 Alloying modulation strategies for zinc anodes.

zinc deposition kinetics by leveraging the electronic structure and crystalline properties of the alloy phases, including dynamically released alloy interfaces and chemically converted alloy layers. For instance, Fang *et al.* proposed an *in situ* interface alloying engineering based on a Ce^{3+}-based additive. Using the specific adsorption of Ce^{3+} at the electrode interface, *in situ* Zn–Ce alloying was achieved, where Zn atoms and Ce atoms formed an alloy interface to inhibit HER and induce the preferential deposition of Zn on the (002) close-packed crystal plane (Fig. 4a). This further improved the cycling stability and reversibility of the zinc anode under a high depth of discharge. The Zn||Zn symmetric battery exhibited high reversibility with uniform Zn/Zn^{2+} plating and stripping (Fig. 4b), and the pouch cells achieved high cathode mass loading and low anode/cathode (N/P) ratio (Fig. 4b). In contrast, the electrolyte showed sluggish ion transfer kinetics, uncontrollable plating/stripping, severe HER, dendrite formation, and random growth upon cycling (Fig. 4c), while the Ce^{3+}-based electrolyte achieved rapid ion transfer kinetics, maintaining stability during long-term cycling (Fig. 4d). The Zn||Zn symmetric battery assembled with the Ce^{3+} additive could cycle stably for 3000 h and reached a cumulative capacity of 27 Ah cm^{-2} at 5 mA cm^{-2}. The full cell with an anode/cathode capacity ratio of 4.3 and a cathode loading of 10 mg cm^{-2} could cycle stably for more than 1000 times at a rate of 2 A g^{-1}.[94]

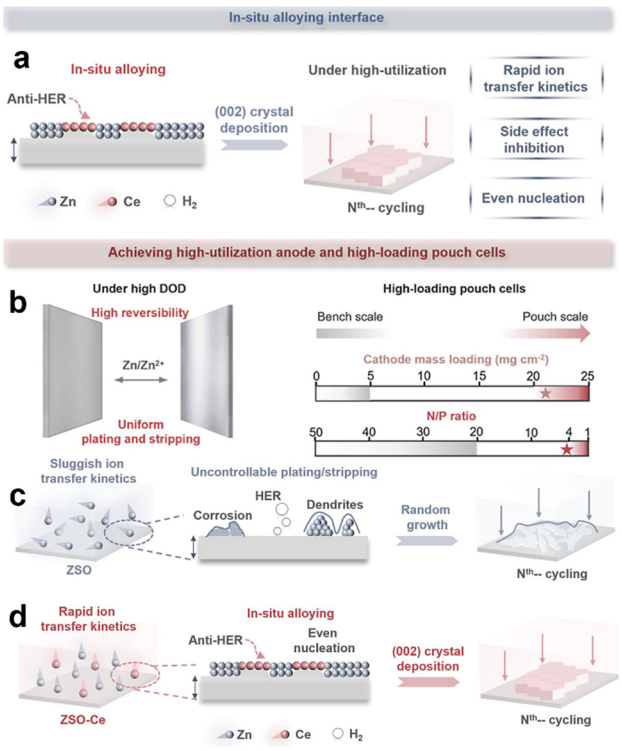

Fig. 4 Schematic diagram of *in-situ* alloying interface (a), high-loading pouch cells (b), schematic of Zn electrodeposition behavior with ZSO electrolyte (c) and ZSO-Ce electrolyte (d), reproduced from ref. 94, with permission from Advanced Functional Materials, copyright 2025.

In terms of dynamically released alloy interfaces, Wu *et al.* proposed a dynamic interfacial alloying strategy. The interface layer prepared by the electrospinning of $SnCl_2$ and polyacrylonitrile can gradually release Sn^{2+}. Since the standard reduction potential of Sn^{2+}/Sn is higher than that of Zn^{2+}/Zn, Sn^{2+} is *in situ* reduced on the anode surface to form Sn. Subsequent zinc deposition promotes the continuous formation of a Zn–Sn alloy, thereby providing the continuous supplementation of zinc-philic sites and the continuous epitaxial growth of the Zn (002) plane. Compared with the Sn-modified Zn anode prepared by a displacement reaction in a $SnCl_2$ solution, this design effectively prevents the failure of zinc-philic sites caused by coverage by Zn. Eventually, the Zn||Zn symmetric battery with the protective layer achieves a low nucleation overpotential of only 0.5 mV and maintains stable cycling for 2000 h at 1 mA cm^{-2}.[95]

For chemically converted alloy layers, Yan *et al.* prepared three types of alloy-coated zinc powders *via* the chemical displacement method, namely Ga–In–Zn (GIZ)-coated zinc, In–Zn (IZ)-coated zinc, and Ga–Zn (GZ)-coated zinc. The results showed that the low Zn^{2+} nucleation barrier on the surface of the Ga–In–Zn alloy promoted uniform ion adsorption and nucleation. Moreover, the migration barrier of the Zn atoms in the Ga–In–Zn alloy phase was significantly lower than that in the pure zinc phase. Among them, the GIZ alloy phase could effectively regulate the migration of Zn^{2+}. In the stripping/plating process, the Zn anodes showed uneven ion transfer (Fig. 5a), while GIZ anodes enabled uniform Zn^{2+} adsorption and deposition; their Zn^{2+} adsorption energies (Fig. 5b) and the surface energies (Fig. 5c) were lower than those of the IZ, GZ and pure Zn anodes. Further, the migration barrier of Zn atoms in the GIZ phase (Fig. 5d) was also significantly lower than that in the IZ and pure Zn phases, thereby promoting zinc-philic ion deposition and inhibiting anode corrosion tendency. The modified GIZ||GIZ symmetric battery achieved stable cycling for more than 3000 h at a current density of 1 mA cm^{-2}.[96] In addition, Zhou *et al. in situ* generated a ZnCo alloy anode on the surface of the zinc metal anode *via* the chemical conversion method. Owing to the strong zinc-philicity of the ZnCo alloy layer, it exhibited fast reaction kinetics during Zn plating/stripping and could effectively avoid dendrite formation caused by the tip effect. Furthermore, linear sweep voltammetry (LSV) and Tafel curves verified that the ZnCo alloy layer effectively improved the corrosion resistance of the bare zinc anode. The ZnCo||ZnCo symmetric battery could cycle stably for more than 2500 h under the test condition of 1.77 mA cm^{-2}.[97]

3.2 Scalable fabrication of the bulk Zn alloy

This strategy targets the entire zinc matrix as its action scope, introducing heterogeneous elements into the zinc bulk phase *via* smelting or electrodeposition to regulate grain boundary structure, reduce atomic migration barriers, and inhibit corrosion. Its core lies in optimizing the intrinsic properties of the entire anode through the uniform distribution of the alloy phases in the bulk, utilizing the integrated structure of the

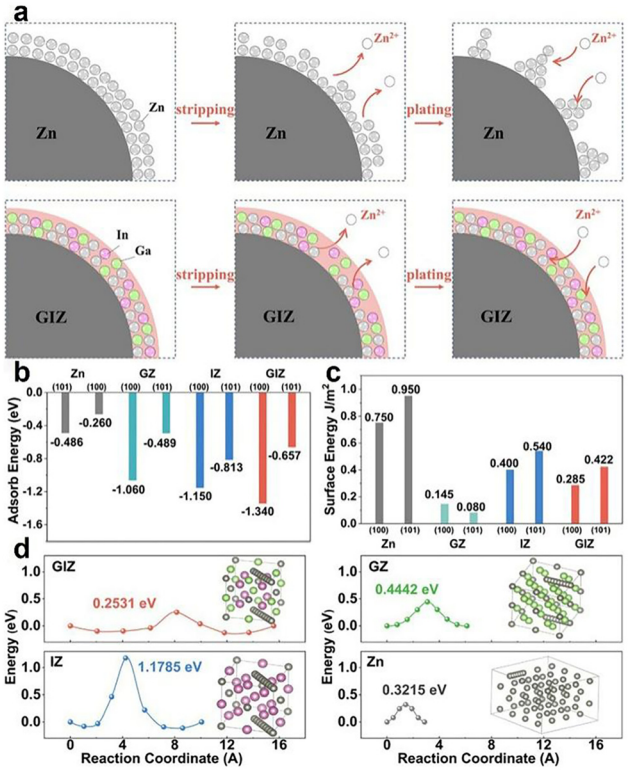

Fig. 5 Schematic of the ion deposition on the Zn and Ga–In–Zn anodes (a), adsorption energies of the Ga–In–Zn, In–Zn, and Zn anodes (b), surface energies of the Ga–In–Zn, Ga–In, In–Zn, and Zn anodes (c), and phase migration energy of the Zn atom in the alloy phases (d), reproduced from ref. 96 with permission from the Advanced Functional Materials, copyright 2025.

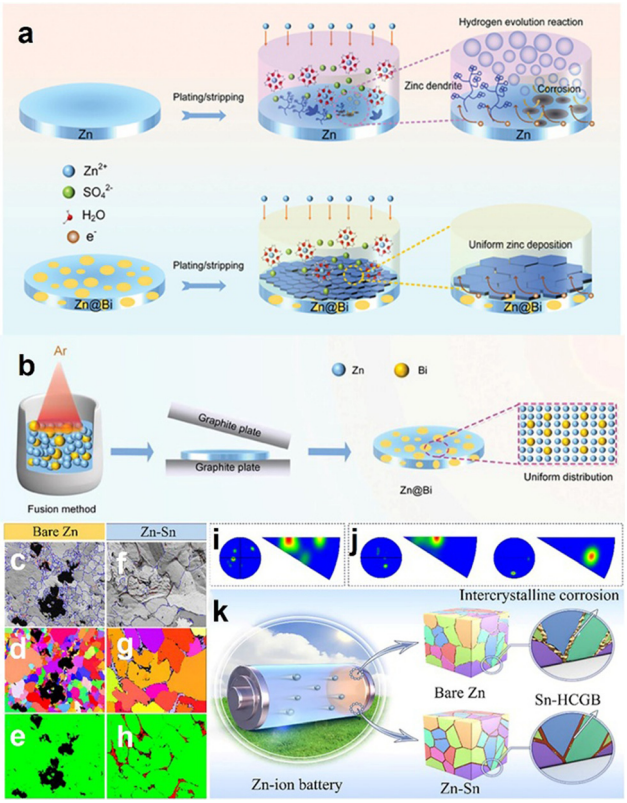

Fig. 6 Deposition mechanism of bare Zn and Zn@Bi (a), post-optimization theoretical computational models for zinc ions with the preparation diagram of Zn@Bi (b), reproduced from ref. 99 with permission from Small, copyright 2023. Schematic of BC + GB after the corrosion of bare Zn (c), IPF mapping image after the corrosion of bare Zn (d), Ph mapping image after the corrosion of bare Zn (e), pole figure and inverse pole figure after the corrosion of bare Zn (f), schematic diagram of BC + GB after the corrosion of the Zn–Sn alloy (g), IPF mapping image after the corrosion of the Zn–Sn alloy (h), Ph image after the corrosion of the Zn–Sn alloy (i), pole figure and inverse pole figure after the corrosion of the Zn–Sn alloy (j), and schematic of the anode grain boundary of bare Zn and Zn–Sn alloy (k), reproduced from ref. 100 with permission from Advanced Functional Materials, copyright 2025.

alloy phases to eliminate interface issues while optimizing electrochemical stability. For example, Wang *et al.* prepared a series of zinc alloys of Zn–Sn, Zn–Al, and Zn–Mn through a smelting-rolling process (smelting at 750 °C under an argon atmosphere, followed by hot-rolling at 300 °C), enabling the large-scale production of alloy sheets with dimensions of 200 × 200 × 0.1 mm^3. High-purity Zn raw materials were used, and low-cost Sn, Al, Mn, and Bi elements modified the grain boundary structure, allowing the added elements to distribute uniformly in the zinc particle bulk phase and form an integrated Zn-based solid solution structure free of interface problems.[98] For example, Liu *et al.* synthesized a zinc-bismuth alloy anode (Zn@Bi) *via* a melting method. In the plating/stripping process, pure Zn anodes suffer from severe HER and zinc dendrite formation and corrosion, while Zn@Bi anodes achieve uniform zinc deposition (Fig. 6a). Its fabrication process involves a fusion method under an Ar atmosphere, followed by processing with graphite plates to obtain Zn@Bi anodes with uniformly distributed Bi in Zn matrix (Fig. 6b). The results showed that Zn@Bi could effectively achieve a uniform anode electric field, thereby regulating the uniform deposition of Zn^{2+} and reducing the formation of zinc dendrites. Theoretical calculations demonstrated that the addition of Bi was beneficial to the stability of the anode structure; high adsorption energy of Zn@Bi corresponded to improved zinc deposition kinetics. When Zn@Bi was paired with an α-MnO_2 cathode to construct a Zn@Bi||MnO_2 battery, it maintained a specific capacity of 119.3 mAh g^{-1} even after 1700 cycles at 1.2 A g^{-1}.[99] Moreover, the Zn–Sn alloy exhibited excellent electrochemical stability and tended to orient along the (002) crystal plane during cycling. The X-ray absorption fine structure (XAFS) results confirmed that Sn elements improved structural stability and inhibited zinc corrosion, mainly because the strong adsorption energy of Sn sites in the Zn–Sn alloy anode for the Zn atoms could suppress dendrite growth.

In addition, Sn elements increased the overpotential of HER, and the uniform Zn–Sn alloy reduced the micro-coupling effect of electrochemical corrosion, optimized electrode potential distribution, and further mitigated corrosion. Compared with Bare Zn (Fig. 6c–e), the Zn–Sn alloy showed a refined grain structure and optimized grain orientation (Fig. 6f–h),

with more uniform ion deposition behavior and suppressed intercrystalline corrosion (Fig. 6i and j). The symmetric battery assembled with this electrode achieved long cycling at 40 mA cm^{-2}; the full cell retained a high reversible capacity of 171 mAh g^{-1} after 10 000 cycles at 2 A g^{-1} (Fig. 6k), significantly outperforming the cycling stability of pure zinc full cells.[100] Moreover, Zn–Ti alloys have been explored by Zhou *et al.*; they proposed a scalable fabrication of the Zn–Ti alloy in order to regulate grain boundary stability and zinc deposition behavior. This method involves introducing Ti into Zn to form intermetallic compounds (IMCs), which preferentially distribute at grain boundaries and remain thermodynamically stable, thereby significantly suppressing intergranular corrosion. Meanwhile, this alloying strategy induces a mixed nucleation and growth mode, reduces the Gibbs free energy for zinc nucleation, and promotes spatially uniform zinc nucleation, ultimately achieving a significantly dense and uniform zinc deposition. These combined advantages enable the Zn–Ti alloy anode to achieve a high zinc reversibility of 99.85% over 4000 cycles, with a stable charge–discharge performance at a current density of 10 mA cm^{-2}, demonstrating excellent cycling stability and electrochemical properties.[101]

Beyond the aforementioned Zn–Sn and Zn@Bi alloys, He *et al.* prepared a zinc–copper alloy anode (Zn@Cu) *via* a melting method. Compared with the bare Zn with dendrite growth, by-products, and H_2 evolution, Zn@Cu achieves smooth and compact Zn deposition along the (002) crystal plane (Fig. 7a and b). The Cu elements in Zn@Cu are uniformly distributed, which significantly mitigates the corrosion issue of the zinc anode in cycled AZIBs. Furthermore, the Zn@Cu alloy prepared by the melting method has a large number of exposed Zn (002) crystal planes on its surface. The Zn@Cu alloy exhibits a high binding energy with Zn atoms, and the abundant nucleation sites restrict the irregular diffusion of Zn^{2+} on the anode surface. The combination of these two effects enables the uniform deposition of Zn^{2+} along the Zn (002) crystal plane, thereby inhibiting dendrite growth. The Zn@Cu||Zn@Cu symmetric battery can operate stably for more than 1000 h. When tested at a current density of 2.0 A g^{-1}, the Zn@Cu||MnO_2 full cell maintains a capacity retention rate of 84.64% after 1000 cycles.[101] In addition, Qiu *et al.* reported an approach to form a zinc anode by alloying zinc with small amounts of Li and Mn, where Li^+ and Mn^{2+} could inhibit the lateral diffusion of Zn^{2+}. Compared with pure Zn with 2D diffusion, nucleation growth, and dendrite formation, the ZnLiMn alloy utilizes an electrostatic shielding mechanism to regulate Zn electrodeposition, achieving uniform Zn deposition (Fig. 7c and d). This process alleviates the formation of zinc-based by-products and zinc passivation. The assembled ZnLiMn||MnO_2 cell could still retain 96% of its capacity after 400 cycles at 1C.[102]

In addition to multi-component bulk alloy design, porous structured bulk alloys have also emerged as an effective strategy. For example, Liu *et al.* fabricated a 3D Zn–W alloy anode *via* a one-step co-electrodeposition method. Compared with Zn foil and 3D Zn–Ag alloy (Fig. 8a–d), the 3D Zn–W alloy exhibits

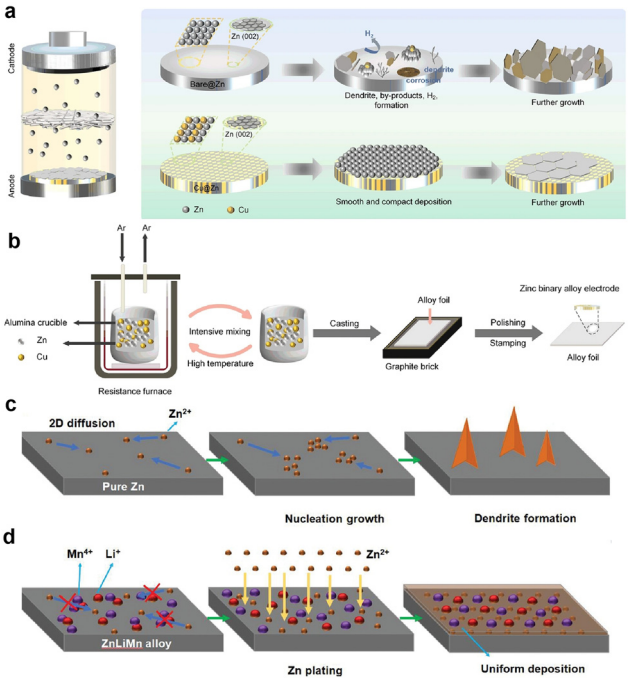

Fig. 7 Schematic of the surface changes of bare@Zn and Cu@Zn (a), process of electrode preparation by the melting method (b), reproduced from ref. 101 with permission from Rare Metals, copyright 2025. Pure Zn faces problems like the uncontrollable 2D diffusion of Zn^{2+} and tip effect, which cause the non-uniform deposition of Zn and dendrite growth, weakening the reversibility of the Zn anode (c). Comparison of the capacity stability and coulombic efficiency of the ZnLiMn-based ZIBs in a long-term cycling test at 1C with those of the Zn||MnO_2 batteries (d), reproduced from ref. 102 with permission from Small, copyright 2022.

stronger H adsorption energy and excellent HER inhibition effect. Its 3D structure enables more uniform Zn^{2+} deposition behavior (Fig. 8e and f) and stable interfacial evolution, with the $ZnWO_4$ phase showing much higher Zn atom adsorption energy than the Zn foil (Fig. 8g–i). This anode exhibits stronger binding energy than the 3D Zn–Ag alloy anode and demonstrates excellent inhibition effect on the HER. The 3D alloy structure increases the active surface area of the anode, enabling stable operation for over 200 h at a high depth of discharge (91.46%) and significantly improving the utilization efficiency of Zn. Compared with the Zn foil with severe HER, dendrite formation, and corrosion (Fig. 8j and k), the 3D Zn-based alloy achieves fast desolvation, even electric field, and suppressed side reactions. The 3D Zn–W||3D Zn–W symmetric battery shows outstanding reversibility during 2400 h of plating/stripping cycles at 1 mA cm^{-2}.[103]

The aforementioned 3D zinc alloy anode has emerged as an effective strategy to promote the uniform deposition of Zn^{2+}. Jiang *et al.* have conducted some explorations; they fabricated a self-supporting 3D porous Zn_xCu_y alloy *via* the *in situ* alloying of Zn and Cu, where the interfacial structure (Fig. 9a) and electrolyte interaction (Fig. 9b) enable dendrite-free zinc stripping/plating. This alloy mainly consists of Zn–Cu intermetallic com-

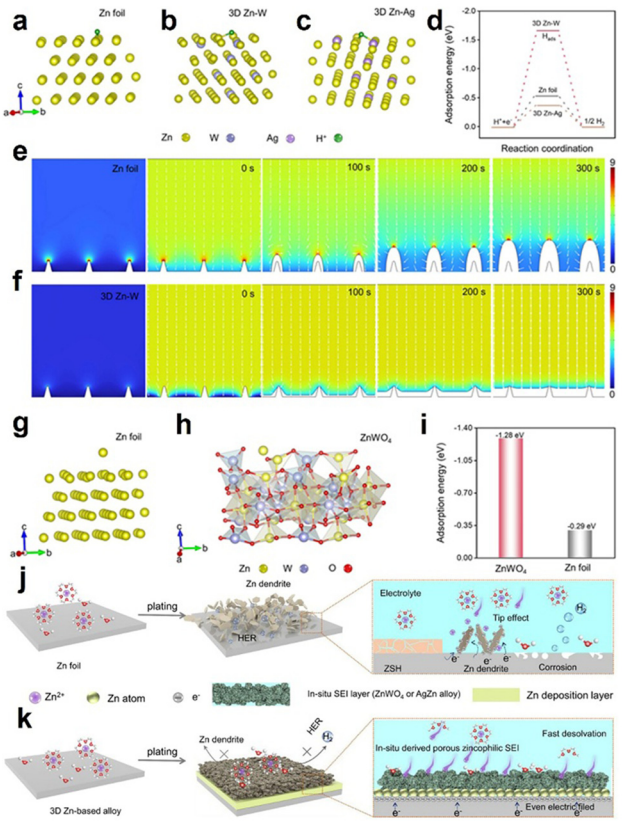

Fig. 8 Adsorption model of H^+ at different anodes on the Zn foil (a), 3D Zn–W (b), and 3D Zn–Ag (c). Corresponding adsorption energy (d). Electric field simulation on the Zn foil (e) and 3D Zn–W anodes (f). Adsorption model of Zn^{2+} at different adsorption sites on the Zn foil surface and (h) $ZnWO_4$ surface (g), and corresponding adsorption energy (i). Schematic of Zn deposition behavior on the Zn foil (j) and 3D Zn alloy anodes (k), reproduced from ref. 103 with permission from Advanced Functional Materials, copyright 2025.

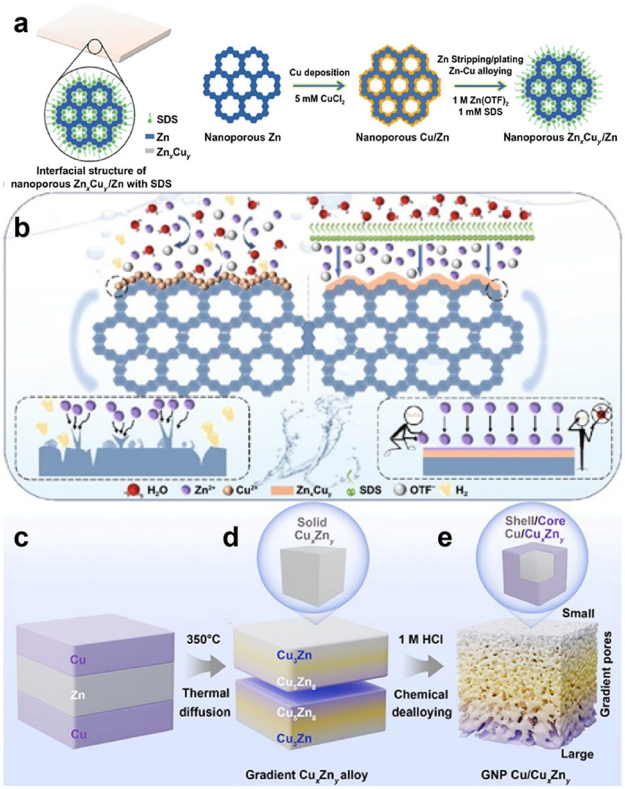

Fig. 9 Schematic of the nanoporous shell/core Zn_xCu_y/Zn sheets that are fabricated by the surface alloying of the Cu and Zn of Cu-decorated nanoporous Zn during sodium dodecyl sulfate-assisted electrochemical Zn stripping/plating cycling (a). Schematic of an anionic surfactant-assisted *in situ* surface alloying method (b), reproduced from ref. 104 with permission from Nano-Micro Letters, copyright 2022. Cu/Zn/Cu sandwich foils (c). Composition-gradient Cu_xZn_y alloy foils produced by the thermal treatment of Cu/Zn/Cu sandwich foils at 350 °C, during which Zn and Cu atoms diffuse into each other (d). GNP Cu/Cu_xZn_y foils consisting of gradient nanopores and shell/core Cu/Cu_xZn_y ligaments, which are formed by selectively etching Zn during the chemical dealloying of gradient Cu_xZn_y alloy precursors in 1 M HCl (e), reproduced from ref. 105 with permission from Nano-Micro Letters, copyright 2025.

pounds (*e.g.*, Cu_5Zn_8 and Cu_3Zn), and the zinc-philic Zn_xCu_y/Zn alloy shell layer guides uniform Zn deposition with zero nucleation overpotential. This enables the self-supporting nanoporous Zn_xCu_y/Zn electrode to exhibit excellent dendrite-free zinc stripping/plating behavior in aqueous electrolytes. The electrode can cycle stably in the electrolyte for more than 1900 h, and the battery assembled with Zn_xCu_y/Zn as the anode and K_2MnO_2 as the cathode material achieves a high specific energy of 430 Wh kg^{-1} and a coulombic efficiency of 99.9%.[104] Later, they further developed a 3D electrode with the gradient composition and structure of nanoporous Cu/Cu_xZn_y *via* an alloying/dealloying process through thermal diffusion and chemical dealloying; a gradient Cu_xZn_y alloy is converted into GNP Cu/Cu_xZn_y with gradient pores and shell/core ligaments (Fig. 9c–e). This electrode consists of interpenetrating gradient nanopore channels and interconnected Cu/Cu_xZn_y shell/core ligaments. The Cu_xZn_y core has a compositional gradient ranging from Cu_5Zn_8 to Cu_3Zn, which ensures unobstructed access to electron and Zn^{2+} transport pathways. Meanwhile, the compositional gradient Cu/Cu_xZn_y shell/core ligaments with a high specific surface area act as zinc-philic sites, guiding the nucleation and deposition of Zn^{2+} from the large-nanopore Cu_5Zn_8 region to the small-nanopore Cu_3Zn region. The AZIBs assembled with this electrode as the anode and carbon cloth-supported $Zn_xV_2O_5$ as the cathode material retain approximately 95% of their capacity after 5000 cycles at 5 A g^{-1}, with a coulombic efficiency of about 99.5%.[105]

3.3 Fabrication of composite coating-based Zn anodes

This strategy integrates alloy phases as non-dynamic functional components into composite systems, combining alloy phases with materials, such as polymers and ceramics, to integrate the zinc-philicity of alloys and the physical barrier function of protective layers, while optimizing ion transport and interface stability. Its core lies in synergistic protection through static collaboration between alloy phases and other components without the dynamic adjustment of the alloy phases. Among relevant

studies, Liu *et al.* designed a robust polymer-alloy artificial protective layer that is a typical implementation of the anode coating modification, which integrates alloy components to enhance both protection and zinc compatibility. By combining SnSb alloy nanoparticles with a Nafion polymer membrane, they achieved a dendrite-free zinc metal anode. Compared with the pure Zn anode, the Nafion-SnSb-modified Zn (NFSS@Zn) anode exhibits a lower nucleation energy barrier, more uniform electric field distribution, and stronger corrosion resistance, effectively suppressing zinc dendrite growth and interfacial side reactions. Bare Zn shows inhomogeneous deposition and dendrite growth, while NFSS@Zn enables homogeneous, dendrite-free deposition (Fig. 10a); its full cell configuration (Fig. 10b) and DFT-calculated adsorption energies (Fig. 10c) further confirm the enhanced stability. Consequently, the NFSS@Zn anode maintains a long cycle life of over 1500 h at 1 mA cm^{-2}, with an ultra-low voltage polarization (25 mV). Meanwhile, when paired with a MnO_2 cathode, the assembled full cell demonstrates stable performance with 1000 cycles at 3 A g^{-1}.[106] In addition, Tian *et al.* constructed a ternary alloy Zn–Sn–Bi interface layer with a 3D structure on zinc metal *via* a simple and universal alloy electrodeposition strategy, forming a composite protective layer that integrates the Zn–Sn–Bi alloy phase with the zinc substrate. Utilizing the synergistic effect of Sn and Bi elements, the Zn–Sn–Bi alloy-modified Zn anode can effectively regulate the nucleation and growth kinetics during zinc deposition and inhibit HER. Combined with DFT calculations, *in situ* optical visualization and spectroscopic analysis, they confirmed that the zinc-philic Zn–Sn–Bi alloy-modified Zn anode has low migration barriers and weak hydrogen adsorption sites (Fig. 10d), which can promote uniform zinc deposition. Consequently, the symmetric battery based on the Zn–Sn–Bi alloy-modified Zn anode can operate stably for 3000 h at a current density of 1.0 mA cm^{-2}, and the average coulombic efficiency of the Zn–Sn–Bi alloy-modified Zn anode||Cu half-cell is close to 100%.[107]

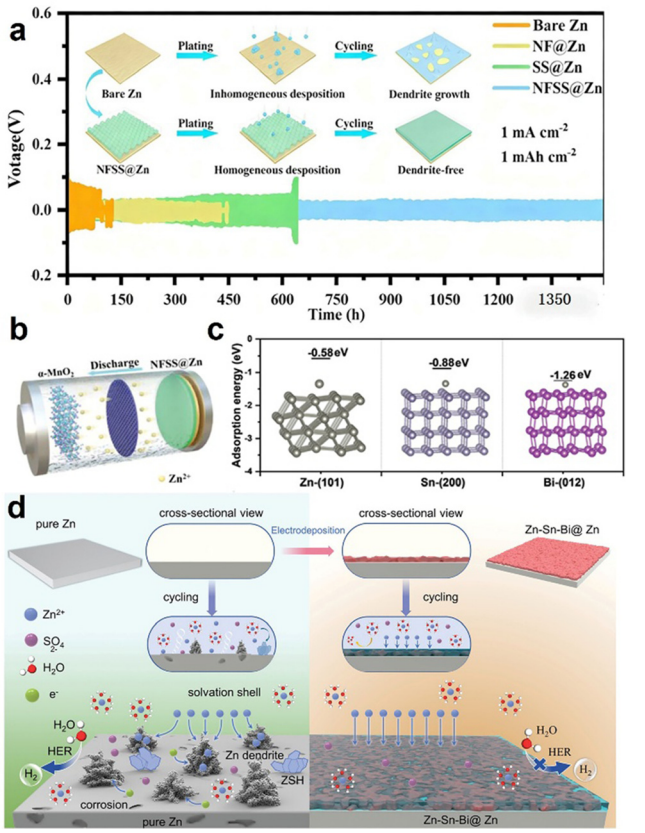

Fig. 10 Schematic showing Zn deposition using bare Zn and NFSS@Zn electrodes, and voltage profiles of symmetric cells with the bare Zn, NF@Zn, SS@Zn, and NFSS@Zn electrodes under the conditions of 1 mA cm^{-2} (a). Schematic of ZIBs (b), reproduced from ref. 106 with permission from Advanced Science, copyright 2023. Adsorption energies and adsorption configurations of a Zn atom on the surfaces of Zn (101), Sn (200), and Bi (012) (c). Schematic of the electrochemical behavior of pure Zn and Zn–Sn–Bi alloy-modified Zn anodes in a 2 M $ZnSO_4$ electrolyte (d), reproduced from ref. 107 with permission from Advanced Functional Materials, copyright 2024.

Notably, Chen's group proposed an alloying strategy based on Bi@ZIF-8 composite coating, constructing a bifunctional interface by depositing ZIF-8-encapsulated nano-Bi particles onto zinc foil *via* a doctor-blading method. The *in situ* alloying effect between Bi and Zn reduces the nucleation barrier, and the ZIF-8 carrier ensures the long-term exposure of alloy active sites. Test results show that the Bi@ZIF-8-modified zinc symmetric cell can stably cycle for 420 h at 7.5 mA cm^{-2}. The Zn–Ni full cell paired with a $Ni(OH)_2$ cathode exhibits a high coulombic efficiency of 98% and retains 80% of its capacity after 2500 cycles. Moreover, the 2 Ah pouch cell based on this modification strategy achieves an energy density of 130 Wh kg^{-1}, demonstrating prominent practical application potential.[108]

Based on this, future research on interface optimization can achieve breakthroughs through primary technical pathways. (1) Employ cross-scale characterization techniques, including *in situ* characterization at the atomic level and synchrotron radiation imaging tests at the mesoscopic scale, to deeply investigate the correlation between interface microstructure and performance, thereby providing a scientific basis for precise interface design. (2) Integrate machine learning technology, utilizing graph neural networks to predict and optimize the optimal interface composition, and strengthen learning algorithms to develop digital models for interface failure prediction, ultimately accelerating material design, research, and development. (3) To address engineering challenges, implement strategies such as solution-based self-assembly, roll-to-roll electrospinning equipment, and the use of biodegradable interface layer materials, aimed at reducing costs, enabling large-scale production, and enhancing environmental compatibility, thereby laying a solid foundation for the industrial application of cathode materials in SSZIBs.

Beyond the above alloy-polymer composite layers, the use of alloy-ceramic composites has become an effective modulation strategy. For example, Mai *et al.* artificially constructed a Ni–Zn intermetallic alloy with solid electrolyte interphase (SEI)-like properties *via* electrodeposition and annealing (Fig. 11a). During the electrode stripping and plating process, the Ni–Zn alloy layer acts as a dynamic barrier at the electrode/electrolyte interface;

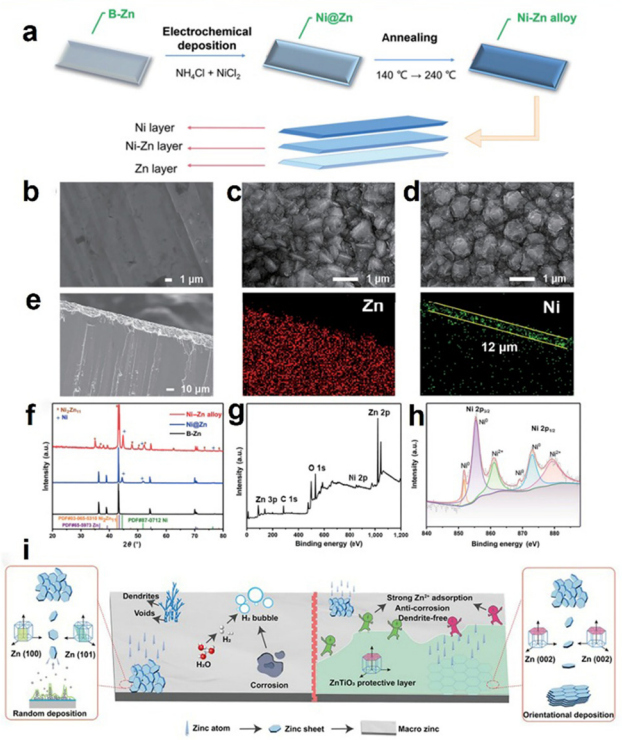

Fig. 11 Schematic of the fabrication procedure and mechanism simulations of Ni–Zn alloy (a). SEM images of B–Zn (b), Ni @Zn (c), and Ni–Zn alloys (d), and the cross-section of Ni–Zn alloy (e). XRD patterns of B–Zn, Ni@Zn, and Ni–Zn alloy (f). XPS spectrum of Ni–Zn alloy (g) and Ni XPS spectrum of Ni–Zn alloy (h), reproduced from ref. 109 with permission from Nano Research, copyright 2022. Schematic of the process of Zn deposition by the designed ZTO coating (I), reproduced from ref. 110 with permission from Advanced Functional Materials, copyright 2025.

Zn atoms migrate out of the zinc electrode bulk during zinc stripping and migrate back into the zinc electrode bulk during plating (Fig. 11b–h). Based on this protection mechanism, the Ni–Zn alloy can guide the horizontal deposition of zinc, inhibiting dendrite formation. The cycle life of the assembled symmetric battery can operate stably for 1900 h at 0.5 mA cm^{-2}.[109] Furthermore, Yi *et al.* constructed a stable and multifunctional insulating coating of zinc titanate (ZTO) on the surface of the zinc anode. This coating can effectively inhibit dendrite formation and zinc anode corrosion. The high degree of matching between ZTO and the Zn (002) crystal plane enables the formation of a stable interface between zinc and ZTO during repeated charge–discharge cycles (Fig. 11i). This coherent interface can regulate the distribution of Zn^{2+} flux, induce the preferentially oriented deposition of zinc along the (002) crystal plane, and ensure the continuity of ion transport. The optimized structure of Zn-ZTO exhibits excellent durability in AZIBs.[110]

3.4 *Ex situ* zinc alloy forming fabrication

This strategy focuses on the pre-fabricated alloy anode architecture, where zinc alloy components are formed through *ex situ* processes, such as melting and mechanical alloying. Its core lies in constructing a stable, homogeneous alloy structure before battery assembly, leveraging the inherent properties of the alloy phase to directly regulate zinc deposition and interface reactions. For example, Zhu *et al.* fabricated a homogeneous ZnNi alloy anode *via* the melting method (Fig. 12a), a typical *ex situ* forming process. The nickel element in the alloy possesses both excellent corrosion resistance and zincophilicity. On the one hand, it significantly reduces the corrosion current of the zinc anode and inhibits the occurrence of corrosion reactions, as well as the formation of by-products. On the other hand, it can homogenize the Zn^{2+} flux and guide the ordered deposition of Zn^{2+} to suppress the growth of zinc dendrites. The symmetric cell assembled with this ZnNi alloy anode achieved a long cycle life of 1000 h at 2 mA cm^{-2}, and the full cell paired with MnO_2 maintained a high capacity retention rate of 90.6% after 1000 cycles.[111] In addition, Cao *et al.* designed an electrochemical-inert liquid Ga–In alloy coating for the Zn anode and fabricated a GaIn@Zn anode *via* *ex situ* processes. As shown in Fig. 12b–d, this unique liquid coating enables inward Zn deposition underneath it, assisted by ultrafast mass and charge transport during charging. The Ga–In alloy coating not only homogenizes Zn^{2+} flux to suppress dendrite growth but also increases the HER overpotential, thereby mitigating Zn anode corrosion. The symmetric cell with this GaIn@Zn anode achieved an ultra-low polarization of 24 mV at 0.25 mA cm^{-2} and an extended cycle life of 2100 h. Furthermore, the full cell paired with MnO_2 retained over 96% of its initial capacity after 48 h of charging. This strategy demonstrates the effectiveness of *ex situ* alloy-based modifications in addressing the interfacial issues of Zn anodes and provides a universal approach for the development of rechargeable metal batteries beyond zinc-storage systems.[112]

3.5 Post-treatment modification of the zinc anode

This strategy targets already-formed zinc anodes, introducing alloying elements or phases through thermal treatment or

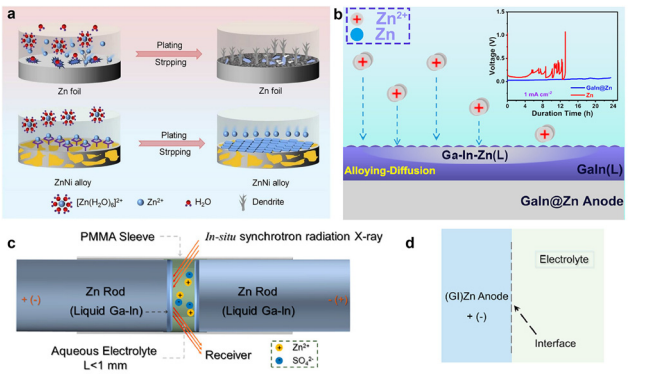

Fig. 12 Preparation of ZnNi alloy (a), reproduced from ref. 111 with permission from Journal of Alloys and Compounds, copyright 2025. Schematic diagram of the Ga–In–Zn(L) anode (b), Model of the home-made separator-free operando symmetric cells (c), Schematic illustration of the anode-electrolyte interface (d), reproduced from ref. 112 with permission from ACS Energy Letters, copyright 2021.

electrochemical modification. Its core lies in optimizing the anode's microstructure after its initial formation, compensating for defects and endowing it with enhanced zincophilicity and suppressed dendrite growth. For example, Chen *et al.* developed a post-treatment thermal infusion strategy for zinc anodes, implementing a melting-wetting-cooling process as the key thermal modification step (Fig. 13a). During this treatment, metallic Zn is densely and firmly encapsulated in the 3D skeleton of the pre-formed anode, which physically constrains the space for dendritic growth and ensures uniform Zn deposition. Meanwhile, they confirmed that the thermal infusion process induces the formation of a ZnO layer on the Zn surface, which effectively inhibits HER and suppresses anode passivation during cycling.[113] The symmetric cell assembled with this anode achieved a long cycling life of over 1000 cycles at 10 mA cm^{-2}. In addition, Kang *et al.* constructed a robust PCL-Nafion@Zn (P–N@Zn)-modified zinc anode *via* an electrochemical-assisted surface modification strategy (Fig. 13b). The modified layer integrates electrospun membranes with a one-piece structure, forming a strong bonding interface with the pristine zinc anode. The Nafion component in the layer is enriched with sulfonic acid groups, which endow the layer with cation selectivity to promote rapid and ordered Zn^{2+} transport, thereby guiding smooth Zn deposition. Benefiting from this synergistic effect, the P–N@Zn||Cu cell achieved a high coulombic efficiency of 99.3% at 2 mA cm^{-2}, and the symmetric cell maintained stable cycling for more than 2900 h at 1 mA cm^{-2}. When applied in full cells, it retained a residual capacity of over 90 mAh g^{-1} after 500 cycles, outperforming bare Zn and single Nafion-modified Zn anodes.[114]

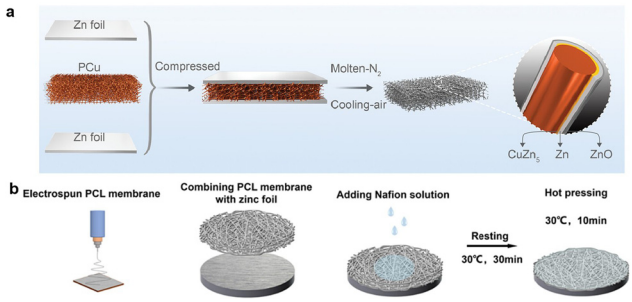

Fig. 13 Schematic of the fabrication of the $CuZn_5$-Zn-ZnO composite material (a), reproduced from ref. 113 with permission from Advanced Materials, copyright 2022. Schematic of the manufacturing process of the modified zinc anode (b), reproduced from ref. 114 with permission from Chemical Engineering Journal, copyright 2024.

4. Conclusions and outlook

4.1 Conclusions

This work summarizes the alloying-dominated performance regulation of high-stability zinc anodes for AZIBs. Through mechanism analysis, strategy classification, and case studies, it clarifies the core value of the alloying strategy in addressing the multi-dimensional stability issues of zinc anodes. To intuitively present the characteristics of different alloying strategies, Table 1 systematically compares the mechanisms, advantages, and limitations of the typical alloying modulation strategies for the Zn anodes.

Beyond the limitations outlined in Table 1, additional potential challenges of these strategies warrant attention for the practical applications of AZIBs. For the *in situ* construction

Table 1 Mechanism, advantages and limitations of the alloying modulation strategies for the Zn anodes

Strategy	Mechanism	Advantages	Limitations
In situ construction of Zn alloy interface	*In situ* formation of an alloy layer to regulate the interfacial charge distribution	Rapid interfacial response; a tight bond with the substrate; little damage to the Zn bulk structure; relatively mild preparation process	Difficult to accurately control the compositional uniformity of the dynamic alloy layer; easy consumption/phase transformation; narrow selection of alloying elements
Scalable fabrication of the bulk Zn alloy	Doping alloying elements into the zinc matrix to regulate the lattice structure and electron density	Long-lasting bulk modification; simultaneous optimization of conductivity, mechanical stability and electrochemical performance; diverse alloying elements for customizable performance; alleviates zinc anode corrosion and pulverization	High-melting-point alloying elements may reduce zinc anode conductivity; complex bulk alloying processes lead to high production cost; excessive alloying elements tend to form second phases; slight reduction in capacity
Fabrication of a composite coating-based Zn anode	Coating alloy phases synergistically inhibit dendrite growth and hydrogen evolution	Direct protection against dendrite growth and corrosion; composite coatings integrate alloy phases' electrochemical inertness and reinforce the phase's structural stability; multifunctional integration *via* coating design	Insufficient interfacial bonding between the coating and zinc matrix; thick coatings may increase interfacial impedance; long-term cycling stability relies on component synergy
Ex situ zinc alloy forming fabrication	Pre-synthesize the alloy particles, then assemble with the Zn substrate	Precise control of alloy composition and structure; stable alloy phase without *in situ* consumption; separable optimization of the alloy and substrate	Poor interfacial contact with Zn substrate; complex pre-synthesis and assembly processes; risk of interface delamination during cycling
Post-treatment modification of the zinc anode	Modify the formed Zn anode to optimize the surface	Low damage to Zn bulk; compatible with mature Zn fabrication processes; flexible regulation of surface properties	Modification effect limited to near-surface; dependence on post-treatment process parameters

of Zn alloy interfaces, the dynamic consumption of alloy layers during long-term cycling may lead to the gradual degradation of the interfacial regulation ability, and the narrow selection of alloying elements further restricts the optimization goal of balancing dendrite inhibition with ionic conductivity. For the scalable fabrication of bulk Zn alloys, high production costs not only stem from complex alloying processes but also from the potential need for post-treatment to eliminate residual internal stresses, accelerating anode pulverization. Moreover, the formation of second phases due to excessive alloying elements may not only reduce the capacity, but also, the phases may act as unintended nucleation sites for Zn dendrites under high current densities. For the fabrication of composite coating-based Zn anodes, the insufficient interfacial bonding can be exacerbated by the volume expansion of Zn during cycling, leading to coating delamination. Meanwhile, thick coatings increase interfacial impedance and may also hinder the rapid transport of Zn^{2+}, compromising the rate performance of the entire battery. Additionally, the long-term cycling stability relying on component synergy implies that minor deviations in coating composition during large-scale production can significantly reduce the consistency of the anode performance.

The main conclusions are as follows. (1) At the mechanism level, alloying synergistically regulates zinc's electronic, crystalline, and interfacial properties *via* atomic interactions with heterogeneous elements. It optimizes Zn^{2+} deposition kinetics, inhibits HER, induces low-surface-energy crystal growth to suppress dendrites, and reduces zinc-electrolyte reactivity. (2) At the strategy level, the alloying approaches with distinct applicability and significant performance gains include interfacial dynamic alloying, bulk alloy optimization, and composite protective layer construction. As detailed in Table 1, each strategy features unique mechanisms, advantages, and limitations. For example, interfacial dynamic alloying enables a rapid response but faces challenges in compositional uniformity control, while bulk alloy optimization achieves long-lasting bulk modification at the cost of potential conductivity reduction and high production costs. (3) At the application level, alloying combines performance advantages with industrial potential. This potential is enabled by mature processes for large-scale production, the use of heterogeneous elements with low cost, and the excellent stability of some alloy anodes under high depth of discharge, supporting large-scale energy storage applications.

4.2 Outlook

Although progress has been made in the alloying strategy, there are still several urgent scientific and technical issues to be addressed. Future research can focus on the following directions (Fig. 14). The first is the dynamic evolution mechanism and the precise regulation of the alloy phases. Current research on the dissolution, reconstruction, and elemental migration of alloy phases during cycling is insufficient. Specifically, potential failure modes are as follows. (1) For solid solution alloys, such as Zn–Sn and Zn–Bi, long-term cycling may lead to inhomogeneous elemental segregation at grain boundaries, resulting in localized corrosion and weakened dendrite suppression. (2) For alloys based on intermetallic compounds, such as Zn–Cu and Zn–Ni, high current densities or acidic electrolyte environments may cause the decomposition of intermetallic phases, thereby leading to the loss of zinc-philic sites and reduced interfacial stability. (3) For porous bulk alloys, such as Zn–W, repeated Zn plating/stripping may trigger the irreversible migration of the alloying elements to the electrode surface, thereby blocking the ion transport channels. To address these issues, it is necessary to combine *in situ* characterization techniques with DFT calculations to reveal the dynamic stability mechanisms of the alloy phases and further develop targeted regulation strategies, such as introducing ultra-thin Al_2O_3 and other interfacial modification layers to inhibit elemental migration or designing multi-component alloy systems like Zn–Sn–Mn to exploit the synergistic effects to stabilize the alloy phase structures.

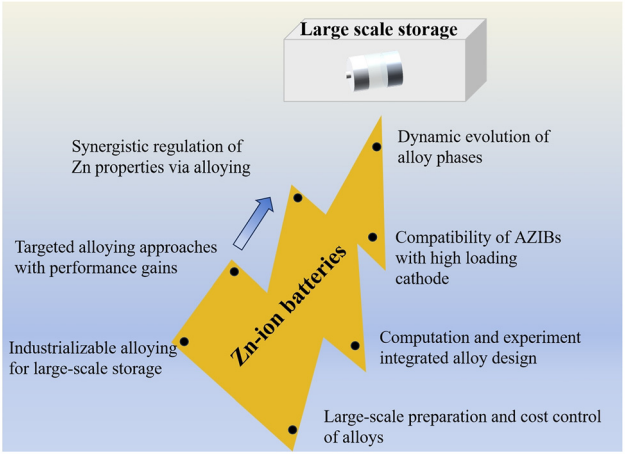

Fig. 14 Future outlook diagram of the alloy anodes for the development of large-scale AZIBs.

The second is the compatibility between high-loading cathodes and full-cell systems. Most studies are based on symmetric cells or low-loading cathodes. However, cathodes with high loadings exceeding 10 mg cm^{-2} will exacerbate challenges in the reaction kinetics and interfacial stability of the Zn anodes. In particular, the increased demand for ion flux may accelerate alloy-phase dissolution and elemental migration, leading to inconsistent anode performance and shortened cycle life of the entire cell. Future research should focus on constructing matching systems between alloy anodes and high-loading cathodes and optimizing electrolyte formulations to simultaneously improve the stability of alloy anodes and the rate performance of high-loading cathodes.

The third is alloy design combining high-throughput calculations and experiments. High-throughput first-principles calculations and machine learning can be used to screen heterogeneous-element combinations with excellent electronic structures, crystalline matching degrees, and chemical stability. The anti-segregation ability can be evaluated by predicting the

binding energy between the alloying elements and the Zn matrix. This will guide experimental synthesis and accelerate the development of high-performance alloy anodes with long-term cycling stability.

The fourth is large-scale fabrication processes and cost control. The existing alloying strategies for Zn alloying are costly, and the uniformity of alloy-phase distribution during large-scale production is also a key issue. It is necessary to develop low-cost, large-scale production technologies, such as continuous rolling and one-step co-electrodeposition, to promote the transition of alloy anodes from laboratory research to industrial applications. To address practical manufacturability challenges, continuous rolling processes can be optimized by adopting low-temperature rolling parameters to avoid excessive energy consumption while ensuring alloy-phase uniformity, which can reduce the risk of grain boundary segregation caused by high-temperature-induced elemental diffusion. Meanwhile, one-step co-electrodeposition can be scaled up using modular electrolytic cells, reducing equipment investment by 30% compared with traditional batch electrodeposition. For cost control, two specific approaches are proposed: (1) selecting low-cost alloying elements, such as Al and Mn, to reduce the raw material costs by 50% while maintaining electrochemical performance and (2) recovering unreacted Zn and alloying elements from production waste through acid leaching and selective precipitation, which can reduce material loss rates to below 5% and further lower overall production costs. In addition, process integration by combining alloy preparation with post-treatments, such as surface passivation, in a single production line can shorten the manufacturing cycle by 20%, improve production efficiency for large-scale deployment, and ensure the consistency and stability of alloy phase structures.

Author contributions

Pushan Guo: literature investigation, writing – original draft. Zhihao Dong: literature investigation, writing – original draft. Jinrong Qi: visualization. Jingjing Yuan: conceptualization. Tao Chen: investigation. Yi Zhang: writing – review & editing. Linhao Xin: supervision, writing – review & editing.

Conflicts of interest

There are no conflicts to declare.

Data availability

No primary research results, software or code have been included, and no new data were generated or analysed as part of this review.

Acknowledgements

The authors gratefully acknowledge the financial support from the Natural Science Foundation of Jiangsu Province (No. BK20231339) and the Changzhou Science and Technology Bureau Project (No. CQ20230095).

References

1 D. Bian, L. Wang, F. Chi, H. Pan, H. Quan and S. Zhu, *Chem. Eng. J.*, 2025, **519**, 164895.
2 H. Chen, W. Huang, Z. Deng, W. Peng, Z. Yang, B. Yuan, L. Yang, S. Li, X. Zheng and Y. Deng, *Adv. Energy Mater.*, 2025, **15**, 2501052.
3 J. Chen, Y. Liu, B. Xiao, J. Huang, H. Chen, K. Zhu, J. Zhang, G. Cao, G. He, J. Ma and S. Peng, *Angew. Chem., Int. Ed.*, 2024, **63**, e202408667.
4 M. Chen, W. Fu, C. Hou, Y. Zhu and F. Meng, *Energy Storage Mater.*, 2025, **80**, 104380.
5 J. Cong, Z. Hu, L. Hu, T. Li, H. Ji, Z. Long, Y. Fan, Z. Wen, Y. C. Lin, H. Xu, Z. Li, S. Li, F. Pan and Y. Huang, *Adv. Funct. Mater.*, 2025, **35**, 2424423.
6 R. Deng, J. Chen, F. Chu, M. Qian, Z. He, A. W. Robertson, J. Maier and F. Wu, *Adv. Mater.*, 2024, **36**, e2311153.
7 R. Deng, Z. He, F. Chu, J. Lei, Y. Cheng, Y. Zhou and F. Wu, *Nat. Commun.*, 2023, **14**, 4981.
8 D. Guo, F. Li and B. Zhang, *Adv. Sci.*, 2025, **12**, e2417323.
9 S. Huang, D. Chen, C. Zheng, H. Zhong, S. Zheng, K. Xu, L. Tang, R. Tang, N. Zhang, Y. Sun and L. Liu, *Chem. Eng. J.*, 2025, **522**, 166855.
10 Z. Huang, S. Yang, Y. Zhang, Y. Zhang, R. Xue, Y. Ma and Z. Wang, *Adv. Energy Mater.*, 2024, **14**, 2400033.
11 H. J. Kim, S. Kim, J. H. Yu, J. H. Lim, H. Yashiro and S. T. Myung, *Chem. Eng. J.*, 2025, **506**, 160017.
12 Y. H. Lee, Y. Jeoun, J. H. Kim, J. Shim, K. S. Ahn, S. H. Yu and Y. E. Sung, *Adv. Funct. Mater.*, 2023, **34**, 2310884.
13 P. Lei, X. Wang, R. Zheng, M. Yang, B. Wang and J. Cheng, *Adv. Funct. Mater.*, 2025, e18756.
14 Y. Lei, F. Liu, L. Chen, M. Xu, Y. Hu, T. Abdiryim, F. Xu, J. You, Y. Tan, Z. Tan and X. Liu, *Nano Energy*, 2025, **143**, 111284.
15 A. Li, J. Hao, K. Wu, C. Chang, X. Zhang, H. Gan, J. Tan, T. Xie, F. Zhou, P. Wang, C. Han, H. Du, B. Li and Q. Liu, *ACS Nano*, 2025, **19**, 13016–13028.
16 N. Hong, G. Liu, H. Zhong, Y. Huang, Y. Kong, C. Liu, H. Li, J. Zeng, T. Liang and X. Qi, *ACS Appl. Mater. Interfaces*, 2025, **17**, 44420–44429.
17 Y. Li, H. Jia, U. Ali, H. Wang, B. Liu, L. Li, L. Zhang and C. Wang, *Adv. Energy Mater.*, 2023, **13**, 2301643.
18 Y. Li, H. Xu, X. Li, X. Lin, H. Zhao, Y. Zhang, K. N. Hui, J. Li and L. Pan, *Adv. Sci.*, 2025, **12**, e07071.
19 C. Li, X. Jiang, H. Qi, D. Chen, T. You, S. Huang, H. Yu, Y. Huang, M. Rao, G. Li, B. Xu, Y. Chen and L. Chen, *Energy Storage Mater.*, 2025, **75**, 104012.

20 Y. Hu, C. Fu, S. Chai, Q. He, Y. Wang, M. Feng, Y. Zhang and A. Pan, *Adv. Powder Mater.*, 2023, **2**, 100093.
21 L. Zhang, J. Xiao, X. Xiao, W. Xin, Y. Geng, Z. Yan and Z. Zhu, *eScience*, 2024, **4**, 100205.
22 S. Guo, L. Qin, J. Wu, Z. Liu, Y. Huang, Y. Xie, G. Fang and S. Liang, *Natl. Sci. Rev.*, 2024, **11**, nwae181.
23 Z. Zhu, S. Xiong, J. Li, L. Wang, X. Tang, L. Li, Q. Sun, Y. Shi and J. Shao, *Batteries*, 2025, **11**, 380.
24 J. Lu, T. Wang, J. Yang, X. Shen, H. Pang, B. Sun, G. Wang and C. Wang, *Angew. Chem., Int. Ed.*, 2024, **63**, e202409838.
25 A. Abbasi, Y. Xu, E. Abouzari-Lotf, M. Etesami, R. Khezri, S. Risse, N. Kardjilov, K. Van Tran, H. Jia, A. Somwangthanaroj, I. Manke, Y. Lu and S. Kheawhom, *Electrochim. Acta*, 2022, **435**, 141365.
26 W. Ma, S. Wang, X. Wu, W. Liu, F. Yang, S. Liu, S. C. Jun, L. Dai, Z. He and Q. Zhang, *Energy Environ. Sci.*, 2024, **17**, 4819–4846.
27 Q. Meng, T. Yan, Y. Wang, X. Lu, H. Zhou and S. Dong, *Chem. Eng. J.*, 2024, **497**, 154541.
28 K. Ouyang, S. Chen, W. Ling, M. Cui, Q. Ma, K. Zhang, P. Zhang and Y. Huang, *Angew. Chem., Int. Ed.*, 2023, **62**, e202311988.
29 G. Qu, Y. Zhao, C. Li, Y. Zhai, Y. Kong, X. He, L. Kong, C. Wang, M. Chen, K. Song, Z. Liu and L. Xu, *Angew. Chem., Int. Ed.*, 2025, **64**, e202422036.
30 R. Li, Y. Du, Y. Li, Z. He, L. Dai, L. Wang, X. Wu, J. Zhang and J. Yi, *ACS Energy Lett.*, 2023, **8**, 457–476.
31 T. Shen, M. Fang, T. Lv, H. Wu, O. Sheng, T. Yang, C. Dong, H. Ji, E. Zhang, X. Zhang, C. Zhang, R. Zheng, J. Zhang and X. Zhang, *Adv. Funct. Mater.*, 2024, **34**, 2408578.
32 C. Wang, X. Wang, H. Wang, C. Zheng, S. Tan, Y. Wang, G. Diao and Z. Jin, *Adv. Funct. Mater.*, 2025, **35**, 2424024.
33 T. Sun, S. Zheng, H. Du and Z. Tao, *Nano-Micro Lett.*, 2021, **13**, 204.
34 D. Guo, F. Li and B. Zhang, *Adv. Sci.*, 2025, **12**, 2417323.
35 B. Xu, Y. Liu, B. Zhao, H. Li, M. Liu, H. Mai and Q. Li, *Molecules*, 2024, **29**, 3416.
36 C.-F. Xiao, Y.-X. Lu, M. Lu, D. Luo, K. Xiao, Y. Wang and Z.-Q. Liu, *Chem. Sci.*, 2025, **16**, 13655–13666.
37 X.-F. Ma, H.-Y. Li, J. Tan, J. Wang, J. Diao, J. Yue, S. Tan, G. Huang, J. Wang and F. Pan, *J. Magnesium Alloys*, 2025, **13**, 1592–1601.
38 H. Wang, S. Deng, S. Wang, W. Li, S. Yuan, J. Han, H. Fu, B. Xu and L. Wei, *Angew. Chem., Int. Ed.*, 2025, **64**, e202422395.
39 M. Wang, Y. Meng, X. Li, J. Qi, A. Li and S. Huang, *Chem. Eng. J.*, 2025, **507**, 160615.
40 K. Wang, S. Li, X. Chen, J. Shen, H. Zhao and Y. Bai, *ACS Nano*, 2024, **18**, 7311–7323.
41 Y. He, Q. Zeng, L. Tang, F. Liu, Q. Li, Y. Yin, S. Xu and B. Deng, *J. Energy Storage*, 2025, **139**, 118725.
42 Q. Wang, J. Zhao, J. Zhang, M. Li, F. Tan, X. Xue, Z. Sui, Y. Zou, X. Zhang, W. Zhang and C. Lu, *Adv. Funct. Mater.*, 2024, **34**, 2405957.
43 X. Wang, L. Liu, Z. Hu, C. Peng, C. Han and W. Li, *Adv. Energy Mater.*, 2023, **13**, 2302927.
44 Z. Wang, J. Dong, K. Zhang, Z. Zhao, Y. Gao, X. Bai, T. Zou, B. Zhao and Y. Wang, *Adv. Funct. Mater.*, 2025, **35**, 2505058.
45 P. Wu, L. Xu, X. Xiao, X. Ye, Y. Meng and S. Liu, *Adv. Mater.*, 2024, **36**, e2306601.
46 X. Wu, Z. Yang, Q. Song, X. Sun, Y. Xu, M. Zhao, X. Li, Y. Yan and M. Chen, *Chem. Eng. J.*, 2024, **497**, 154395.
47 J. Yan, M. Cen, Y. Guo, B. Wang, Y. Tian, Z. Song, X. Peng, J. Lian and D. H. L. Ng, *J. Mater. Sci.*, 2025, **60**, 19883–19895.
48 H. Qi, C. He, C. Song, J. Gao, Q. Gao, W. Luo, Z. Zhang, H. Liu, X. Yuan, W. Wu, B. Zhao, L. Kong, Y. Cheng and L. Guo, *Chin. Chem. Lett.*, 2025, **36**, 111591.
49 Y. Xia, R. Tong, J. Zhang, M. Xu, G. Shao, H. Wang, Y. Dong and C. A. Wang, *Nano-Micro Lett.*, 2024, **16**, 82.
50 T. Han, C. Zhang and J. Luo, *Langmuir*, 2018, **34**, 11281–11291.
51 X. P. Jiang, W. Yu, Y. Wei, H. J. Wu, J. P. Ding, C. Y. Hu, X. J. Liu, J. Feng and X. Y. Chong, *Rare Met.*, 2025, **44**, 9036–9052.
52 F. Xiao, X. Wang, K. Sun, Q. Zhao, C. Han and H.-F. Li, *Chem. Eng. J.*, 2024, **489**, 151111.
53 Y. Xiao, J. Ren, M. Li, K. Xiao and Y. Wang, *Chem. Eng. J.*, 2023, **474**, 145801.
54 W. Xie, K. Zhu, H. Yang and W. Yang, *Adv. Mater.*, 2024, **36**, e2306154.
55 Y. Yang, L. Qin, Q. He, C. Yin, Y. Lei, S. Liang and G. Fang, *Sci. Bull.*, 2025, **70**, 104–124.
56 C. You, R. Wu, X. Yuan, L. Liu, J. Ye, L. Fu, P. Han and Y. Wu, *Energy Environ. Sci.*, 2023, **16**, 5096–5107.
57 Y. Yuan, Z. Li, R. Deng, S. D. Pu, M. Walker, M. Cai, F. Wu, P. G. Bruce and A. W. Robertson, *Energy Environ. Sci.*, 2025, **18**, 5610–5621.
58 J. Yue, S. Chen, J. Yang, S. Li, G. Tan, R. Zhao, C. Wu and Y. Bai, *Adv. Mater.*, 2024, **36**, e2304040.
59 J. Zhang, L. Mao, Z. Xia, M. Fan, Y. Deng and Z. Chen, *Adv. Funct. Mater.*, 2024, **35**, 2412547.
60 J. Zhang, M. Shi, H. Gao, X. Ren, J. Cao, G. Li, A. Wang and C. Liu, *Chem. Eng. J.*, 2024, **491**, 152050.
61 S. Zhang, Y. Jin, J. Yang, D. Zhang, Z. Gao, X. Wu, X. Zhang, J. Qin and J. Cao, *Chem. Eng. J.*, 2025, **521**, 166871.
62 X. Zhang, L. Zhang, X. Jia, W. Song and Y. Liu, *Nano-Micro Lett.*, 2024, **16**, 75.
63 Y. Zhang, S. Shen, Z. Kang, N. Gao, D. Yin, L. Zhao, B. Wen, T. Deng, K. Xi, Y. Su, H. Zhao and S. Ding, *Energy Environ. Sci.*, 2025, **18**, 3668–3679.
64 G. Liu, B. Fu, Z. Liu, L. Li, S. Liang and G. Fang, *Rare Met.*, 2024, **43**, 5005–5016.
65 L. L. Zhao, S. Zhao, N. Zhang, P. F. Wang, Z. L. Liu, Y. Xie, J. Shu and T. F. Yi, *Energy Storage Mater.*, 2024, **71**, 103628.
66 Q. Zhao, H. Wang, G. Chen, J. Chen, S. Wang and X. Rao, *Energy Storage Mater.*, 2025, **80**, 104442.

67 Z. Zhu, F. Cai and J. Yu, *Ionics*, 2016, **22**, 1353–1359.
68 Z. Zhao, R. Zhang, Z. Li, J. Sun, X. Zhou, Z. Yan, L. Li and X. Chen, *Energy Storage Mater.*, 2025, **81**, 104521.
69 L. F. Zhou, Y. J. Gao, T. Du, L. Y. Liu, Y. S. Wang, H. Jia and J. Z. Wang, *Cell Rep. Phys. Sci.*, 2025, **6**, 102565.
70 M. Zhang, J. Fu, N. Xu and L. Meng, *Chem. Eng. J.*, 2025, **511**, 161944.
71 M. Zhu, H. Wang, H. Wang, C. Li, D. Chen, K. Wang, Z. Bai, S. Chen, Y. Zhang and Y. Tang, *Angew. Chem., Int. Ed.*, 2024, **63**, e202316904.
72 Y. Fu, V. Yousefi Mehr, M. R. Toroghinejad, X. Chen, J. Jie and S. Zhu, *J. Mater. Res. Technol.*, 2025, **34**, 2127–2132.
73 W. Chen, H. Hou, Y. Zhang, W. Liu and Y. Zhao, *J. Mater. Res. Technol.*, 2023, **24**, 8401–8413.
74 Y. Zhu, H. Li, Y. Rao, S. Guo and H. Zhou, *Adv. Energy Mater.*, 2024, **14**, 2303928.
75 Y. Zhu, G. Liang, X. Cui, X. Liu, H. Zhong, C. Zhi and Y. Yang, *Energy Environ. Sci.*, 2024, **17**, 369–385.
76 M. Guo, P. Ma, L. Wei, J. Wang, Z. Wang, K. Zheng, D. Cheng, Y. Liu, H. Dai, G. Guo, E. Duan and J. Deng, *J. Am. Chem. Soc.*, 2023, **145**, 11110–11120.
77 X. Zhang, A. Dong, H. Gao, G. Wang, Y. Yin, L. Che and H. Gao, *Nanomaterials*, 2025, **15**, 1319.
78 H. Li, Z. Liu, Y. Tang, S. Liang and G. Fang, *cMat*, 2024, **1**, e25.
79 B. Zhu, J. Tang, Z. Yao, J. Cui, Y. Hou, J. Chen, L. Tang, Y. Fu, W. Zhang and J. Zhu, *Chem Bio Eng.*, 2024, **1**, 381–413.
80 Y. Yan, C. Shu, T. Zeng, X. Wen, S. Liu, D. Deng and Y. Zeng, *ACS Nano*, 2022, **16**, 9150–9162.
81 H. Lu, D. Zhang, Z. Zhu, N. Lyu, X. Jiang, C. Duan, Y. Qin, X. Yuan and Y. Jin, *Adv. Sci.*, 2024, **11**, 2401575.
82 J. Cao, M. Sun, D. Zhang, Y. Zhang, C. Yang, D. Luo, X. Yang, X. Zhang, J. Qin, B. Huang, Z. Zeng and J. Lu, *ACS Nano*, 2024, **18**, 16610–16621.
83 Z. Shi, M. Yang, Y. Ren, Y. Wang, J. Guo, J. Yin, F. Lai, W. Zhang, S. Chen, H. N. Alshareef and T. Liu, *ACS Nano*, 2023, **17**, 21893–21904.
84 X. Hu, H. Dong, N. Gao, T. Wang, H. He, X. Gao, Y. Dai, Y. Liu, D. J. L. Brett, I. P. Parkin and G. He, *Nat. Commun.*, 2025, **16**, 2316.
85 D. Zhang, Z. Song, L. Miao, Y. Lv, L. Gan and M. Liu, *Chem. Sci.*, 2024, **15**, 4322–4330.
86 X. Zhu, W. Zhang, Z. Peng, L. Pan, B. Li, Z. Zhang, J. Zhu, W. Meng, L. Dai, L. Wang and Z. He, *Chem. Eng. J.*, 2024, **499**, 156521.
87 T. Wang, Q. Xi, Y. Li, H. Fu, Y. Hua, E. G. Shankar, A. K. Kakarla and J. S. Yu, *Adv. Sci.*, 2022, **9**, 2200155.
88 Y. Zhou, G. Li, S. Feng, H. Qin, Q. Wang, F. Shen, P. Liu, Y. Huang and H. He, *Adv. Sci.*, 2022, **10**, 2205874.
89 Y. Li, J. Y. Wang, J. W. Yin, P. F. Wang, Z. L. Liu, J. Shu and T. F. Yi, *Energy Storage Mater.*, 2025, **75**, 104056.
90 M. Lin, R. Qi, W. Zhang, Z. Ren, J. Si, Q. Lei, Y. Sun, H. Li, J. He, Q. Zhang, J. Zeng, W. Wen, Y. Gao, X. Li and D. Zhu, *Adv. Energy Mater.*, 2024, **14**, 2401288.
91 K. Liu, M. Sun, S. Yang, G. Gan, S. Bu, A. Zhu, D. Lin, T. Zhang, C. Luan, C. Zhi, P. Wang, B. Huang, G. Hong and W. Zhang, *Adv. Energy Mater.*, 2024, **14**, 2401479.
92 T. Wang, X. Li, Z. Li, T. Liu, X. Wang, A. Devaraj, C. A. Powell and J. F. dos Santos, *Nat. Commun.*, 2024, **15**, 10664.
93 Z. Liu, X. Li, Z. Li, L. Ma, Y. Wang, C. Ye, M. Ye and J. Shen, *Chem. Eng. J.*, 2024, **479**, 147412.
94 X. Bu, M. Li, Z. Liu, S. Liang and G. Fang, *Adv. Powder Mater.*, 2025, **4**, 100332.
95 X. Wang, W. Fan, Y. Dong, H. Huang, L. An and J. Wu, *Adv. Funct. Mater.*, 2025, e16514.
96 Q. Li, C. Fang and C. Yan, *Adv. Funct. Mater.*, 2025, 2509192.
97 L. Jiang, Y. Chai, D. Ji, L. Li, L. Li, B. Lu, D. Li and J. Zhou, *Green Energy Environ.*, 2025, **10**, 382–389.
98 Z. Zhao, Y. Liao, S. Li, B. Xu, Q. Liu, Y. Zhang, Y. Huang and J. Wang, *Adv. Funct. Mater.*, 2025, e20763.
99 Y. Du, Y. Feng, R. Li, Z. Peng, X. Yao, S. Duan, S. Liu, S. C. Jun, J. Zhu, L. Dai, Q. Yang, L. Wang and Z. He, *Small*, 2024, **20**, e2307848.
100 B. Xiao, J. Chen, C. Hu, L. Mou, W. Yang, W. He, Z. Lu, S. Peng and J. Huang, *Adv. Funct. Mater.*, 2023, **33**, 2211679.
101 J. Zhu, L. Wu, Z. Peng, S. Li, X. Li, Z. Zhang, N. Zhao, B. Li, W. Meng, L. Wang, L. Dai and Z. He, *Rare Met.*, 2025, **44**, 6092–6101.
102 Y. Zhang, X. Yang, Y. Hu, K. Hu, X. Lin, X. Liu, K. M. Reddy, G. Xie and H. J. Qiu, *Small*, 2022, **18**, e2200787.
103 M. Lu, B. H. Xiao, Y. X. Lu, K. Xiao and Z. Q. Liu, *Adv. Energy Mater.*, 2025, **15**, 2500785.
104 J. Liu, J. H. Jia, L. B. Chen, H. Meng, Q. Ran, H. Shi, G. F. Han, T. H. Wang, Z. Wen, X. Y. Lang and Q. Jiang, *Nano Lett.*, 2025, **25**, 4298–4306.
105 H. Meng, Q. Ran, T. Y. Dai, H. Shi, S. P. Zeng, Y. F. Zhu, Z. Wen, W. Zhang, X. Y. Lang, W. T. Zheng and Q. Jiang, *Nano-Micro Lett.*, 2022, **14**, 128.
106 J. Duan, J. Dong, R. Cao, H. Yang, K. Fang, Y. Liu, Z. Shen, F. Li, R. Liu, H. Li and C. Chen, *Adv. Sci.*, 2023, **10**, e2303343.
107 Y. Xin, J. Qi, H. Xie, Y. Ge, Z. Wang, F. Zhang, B. He, S. Wang and H. Tian, *Adv. Funct. Mater.*, 2024, **34**, 2403222.
108 J. He, W. Zhou, J. Li, S. Chen, D. Zhu and Y. Chen, *Chem. Eng. J.*, 2024, **485**, 149740.
109 Y. Li, Y. H. Zhao, J. Wang, D. Xu, Y. Wang, P. Wang, Z. Liu, Q. Lai, J. Shu, Q. Zhang and T. F. Yi, *Adv. Funct. Mater.*, 2025, e09963.
110 J. Chen, Y. Zhu, F. Zhang, Y. Wang, W. Xu, Y. Zhang, L. Shi, X. Qiang, Y. Ma and J. Zhao, *Nano Res.*, 2025, **18**, 94907224.
111 X. Zhu, W. Zhang, M. Zhang, L. Yu, B. Li, J. Cheng, L. Pan, Z. Peng, S. Li, B. Li, Z. Zhang, L. Dai, L. Wang, N. Zhao and Z. He, *J. Alloys Compd.*, 2025, **1005**, 176159.

112 C. Liu, Z. Luo, W. Deng, W. Wei, L. Chen, A. Pan, J. Ma, C. Wang, L. Zhu, L. Xie, X. Cao, J. Hu, G. Zou, H. Hou and X. Ji, *ACS Energy Lett.*, 2021, **6**, 675–683.
113 J. Zhou, F. Wu, Y. Mei, Y. Hao, L. Li, M. Xie and R. Chen, *Adv. Mater.*, 2022, **34**, 2200782.
114 J. Ju, Y. Zhang, Y. Zhang, Z. Zhang, S. Chen, C. Zhao and W. Kang, *Chem. Eng. J.*, 2024, **481**, 148479.